Asymmetry in the effect of magnetic field on photon detection and dark counts in bended nanostrips

A. Semenov,[1] I. Charaev,[2] R. Lusche,[1] K. Ilin,[2] M. Siegel,[2] H.-W. Hübers,[1,3] N. Bralović,[4] K. Dopf,[4] and D. Yu. Vodolazov[5,6]

[1]*Institute of Optical Sensor Systems, German Aerospace Center (DLR), Rutherfordstraße 29, 12489 Berlin Germany*

[2]*Institute of Micro- and Nanoelectronic Systems, Karlsruhe Institute of Technology (KIT), Hertzstraße 16, 76187 Karlsruhe, Germany*

[3]*Humboldt-Universität zu Berlin, Department of Physics, Newtonstraße 15, 12489 Berlin, Germany*

[4]*Light Technology Institute (LTI), Karlsruhe Institute of Technology (KIT), Kaiserstraße 12, 76131 Karlsruhe, Germany*

[5]*Institute of Physics of Microstructures, Russian Academy of Sciences, 603950 Nizhny Novgorod, GSP-105, Russia*

[6]*Lobachevsky State University of Nizhny Novgorod, 23 Gagarin Avenue, 603950 Nizhny Novgorod, Russia*

(Received 22 July 2015; revised manuscript received 4 September 2015; published 17 November 2015)

Current crowding in the bends of superconducting nanostructures not only restricts measurable critical current in such structures, but also redistributes local probabilities for the appearance of dark and light counts. Using structures in the form of a square spiral, where all bends have the same symmetry with respect to the directions of the bias current and external magnetic field, we have shown that areas around the bends largely contribute to the rate of dark counts and to the rate of light counts at small photon energies. The minimum in the rate of dark counts reproduces the asymmetry of the maximum in the critical current as a function of the magnetic field. Contrarily, the minimum in the rate of light counts demonstrates opposite asymmetry. The rate of light counts becomes symmetric at large currents and fields. Comparison of the computed local absorption probabilities for photons and the simulated local threshold detection current reveal the areas near bends that deliver the asymmetric rate of light counts. Asymmetry in count rates is absent in circular spirals without bends.

DOI: 10.1103/PhysRevB.92.174518 PACS number(s): 74.25.Ha, 74.78.−w, 85.25.Oj, 78.67.Uh

I. INTRODUCTION

Meandering nanometer-wide superconducting strips are commonly used for detection of single photons in the near-infrared spectral range [1]. Statistical fluctuations in the form of dark counts restrict the minimum detectable photon flux. Recently, it has become clear that, in strips with bends, current crowding limits the achievable supercurrent to a value noticeably lower than the depairing current in straight fragments of these strips [2]. At the inner edges of bends and turns, where the supercurrent rounds a sharp corner, local current density increases, which causes a local reduction of the free energy barrier for nucleation of magnetic vortices. Among different topological fluctuations, hopping of vortices across the strip is commonly considered as a mechanism of dark counts [3–5]. Hence, bends and turns with sharp corners are places from which dark counts most probably come. Only a few indirect experimental verifications of this supposition have been reported. Engel *et al.* [5] found in their meanders a slight asymmetry in the rate of dark counts with respect to the magnetic field direction and assigned it to differences in shapes of right and left turns. Akhlaghi *et al.* [6] showed that, in a nanowire with a single bend, rounding the sharp inner corner of the bend results in an increase of the critical current and in a reduction of the dark count rate (DCR) of the whole structure. Lusche *et al.* [7] found differences in current dependencies of the vortex energy barrier in the case of light and dark counts and associated them with different locations of these events.

Light counts in narrow strips are related to either current- or fluctuation-assisted vortex crossing. In the first deterministic scenario, a photon creates a hotspot in the strip, which forces the current density to redistribute around the absorption site. A vortex nucleates at any point where, after current redistribution, the velocity of the superconducting condensate locally achieves its critical value [8]. This can be either a single vortex near the strip edge or a vortex-antivortex pair (VAP) close to the midline of the strip. Vortices are then swept by the Lorentz force across the strip. The energy dissipated along the trajectory of the vortex in the strip causes the formation of a normal belt. In the fluctuation-assisted scenario, a vortex crosses, with certain thermodynamic probability, the entire strip through the segment where the energy barrier is reduced due to photon absorption [9,10]. Discovering the local nature of count events has made it possible to bridge these two scenarios in the framework of the deterministic model. Studies of the effect of the external magnetic field on the light count rate [5,7] have shown that the energy barrier depends differently on the current for low and high energy photons and that the variation of the barrier with the photon energy noticeably deviates from the model predictions for straight strips [9]. These inconsistencies are due to simplifications of the boundary conditions in the model of Ref. [9]. They could be partly relaxed by suggesting different locations of light counts for photons with different energies [7].

However, strips in the common meander form prevent one from figuring out where count events occur. Differentiating contributions from straight portions and bends by applying a magnetic field runs into the problem that the meander has bends with a different symmetry with respect to the directions of the current flow and magnetic field. Chirality, i.e. the dual symmetry of turns in the meander, masks the expected asymmetry in magnetic fields for count events that occur in bends. Using single bends and bridges helps solve the problem but has its own complications, such as resonance effects in the absorption probability for particular wavelengths and current crowding imposed by closely spaced contacts. Furthermore, optical coupling to small structures is deteriorated.

In this paper, we studied specially designed square-shaped spirals that contain bends with the only one symmetry with respect to current and magnetic field directions and have an optical coupling efficiency comparable to the meandering strips. As a reference, we used circular spirals without bends.

We show that, in accordance to a common understanding of the current crowding effect in magnetic fields [11–13], the magnetic field dependences of the critical current in square spirals are nonsymmetric and that this asymmetry is reversible with either current or field direction. We demonstrate that there is no asymmetry in field dependences of the critical current and count rates in bend-free spirals. Contrary, in square spirals, there exists an asymmetry in the field dependences of rates of dark and light counts. Invoking handedness of the observed asymmetries and mapping the computed local absorption probability for photons and the local detection threshold current, we identify areas in the bends where, at low photon energies, light counts occur.

In the next section, we describe the manufacturing process of spiral structures and their characterization. We describe the experimental findings in a separate section, which is followed by the section with the theoretical model. Simulation results for the local absorption probability and discussion are presented in the last section.

II. TECHNOLOGY AND EXPERIMENTAL DETAILS

Spiral structures were prepared from niobium nitride (NbN) films on sapphire substrates. We started by depositing a thin NbN film on an R-plane cut, one-side polished substrate via reactive magnetron sputtering of a pure Nb target in an argon and nitrogen atmosphere. Partial pressures of argon and nitrogen were $P_{\mathrm{Ar}} = 1.9 \times 10^{-3}$ mbar and $P_{\mathrm{N2}} = 4 \times 10^{-4}$ mbar, respectively. During deposition, the substrate was placed without being thermally anchored on the surface of a holder, which was freely laid on a heater plate. The plate was kept at a temperature of 850 °C. The film thickness $d = 4.8 \pm 0.2$ nm was measured with a profilometer. A detailed description of the deposition process of NbN thin films can be found elsewhere [14]. We have chosen two designs of spirals for our experiment: the circular, Archimedean spiral [Fig. 1(a)] and the square spiral, which is also called an Egyptian or Greek spiral [Fig. 1(b)]. All spirals had one contact pad outside of the spiral and one in the geometric center. The pad in the center was in the form of either a circle for the circular spiral or a square for the square spiral with a diameter of 1.2 μm or sizes $1.3 \times 1.3\,\mu\mathrm{m}^2$, respectively. The geometric parameters of the spirals were measured with a scanning electron microscope (SEM). The SEM images of spirals are shown in Fig. 1. All spirals reported here have a strip width $w = 110 \pm 5$ nm and a strip spacing of 100 nm, which both define a geometric filling factor of approximately 50%. All bends in square spirals have nominally the same rounding radius $r = 71 \pm 5$ nm at their inner corners. The fabrication process of a spiral specimen includes three steps. To pattern the NbN film into the spiral, we used electron-beam (e-beam) lithography over polymethyl methacrylate (PMMA) resist with a thickness of about 65 nm. The transfer of the image, created in the resist, was made by a subsequent milling with Ar ions at a pressure of 1.1×10^{-4} mbar. We used a radio frequency (RF) plasma source with a 100 mm diameter from the firm Nordiko. At the Ar gas flow of 4.8 sccm, 200 W of RF power, and 400 V of the ion-accelerating voltage, we achieved an etching rate of 1.6 nm/min for our NbN films.

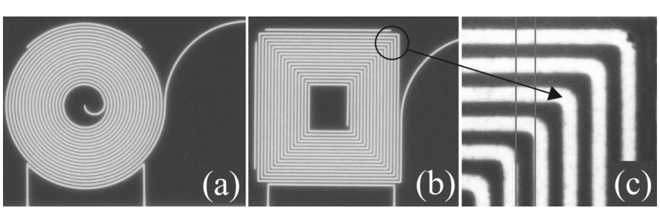

FIG. 1. SEM images of (a) a circular spiral and (b) a square spiral. Dark color represents strips and surrounding fields from NbN film. The outer diameter of the Archimedean spiral is 7.3 μm. The size of the square spiral is $6.5 \times 6.5\,\mu\mathrm{m}^2$. (c) Corner rounding in bends of the square spiral. The distance between two vertical cursor lines is 112 nm. Irregularities at the edge of the NbN field that surrounds the spiral do not affect the critical current of the strip.

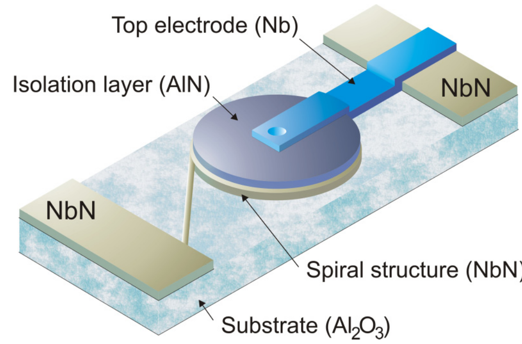

FIG. 2. (Color online) Schematic of the multilayer structure with the top electrode.

To lead bias current through, the spiral was isolated from the top except for the central pad and then a top electrode was brought above the isolating layer. The schematic of the contacting and isolating layers is shown in Fig. 2. At the second step, we made the isolating layer from aluminum nitride (AlN). A new PMMA layer was spun over the spiral and the ring with an outer diameter slightly larger than the outer diameter of the spiral and the inner diameter slightly smaller than the size of the central contact pad was opened. We further deposited 50 nm of AlN at room temperature by reactive magnetron sputtering of pure Al target in an argon and nitrogen atmosphere at partial pressures $P_{\mathrm{Ar}} = 3 \times 10^{-3}$ mbar and $P_{\mathrm{N2}} = 4.5 \times 10^{-3}$ mbar, respectively. After deposition, AlN from the central pad and from the area surrounding the spiral was removed in warm acetone via liftoff. The 50 nm layer of AlN reliably isolates the spiral structure from being short cut by the top electrode. The last step in the fabrication of spiral specimens was processing of the top contact. To ensure a proper electrical contact to the spiral, the top electrode must be at least two times thicker than the isolating layer. The top electrode was formed by e-beam lithography from a 100-nm-thick Nb superconducting film, which was deposited on top of the isolating layer by magnetron sputtering of pure Nb in an argon atmosphere at an argon pressure of $P_{\mathrm{Ar}} = 5 \times 10^{-3}$ mbar. For e-beam lithography, we used PMMA resist with a thickness of 120 nm.

We measured the temperature dependence of the resistance of our spirals in the range from room temperature down to 4.2 K using a standard four-probe technique. The critical temperature T_C was defined as the lowest temperature at which

TABLE I. Parameters of two typical spiral structures from NbN films: *RRR*, residual resistance ratio, i.e. the ratio of the resistance of the structures at room temperature to that at 20 K; I_C (4.2 K), critical current at 4.2 K.

Type	w [nm]	d [nm]	RRR	T_C [K]	I_C (4.2 K) [μA]
Circular spiral	104	4.8	0.98	11.7	35
Square spiral	112	4.8	0.97	11.9	36

a nonzero resistance could be measured. We found $T_C \approx 12$ K for all our samples with a variation from sample to sample of less than 0.3 K. Samples with a smaller strip width typically have a lower critical temperature [15,16]. The current-voltage (CV) characteristics of the samples were measured in the current-bias mode at 4.2 K. The critical current I_C of the spiral structures was associated with the well-pronounced jump in the voltage from zero to a finite value corresponding to the normal state. The parameters of studied structures are listed in Table I.

Measurements in magnetic field were performed in the homemade inset with a thermally isolated capsule for specimens, where the temperature could be varied between 2 and 15 K. The magnetic field up to 2 T was provided by a superconducting solenoid. Light from a monochromator was fed to the samples via a multimode optical fiber. We did not control light polarization which was slightly elliptical. Electrical readout was made via coaxial cable. For more details of the experimental setup, see Ref. [7]. We checked that the DCR down to approximately 10^{-1} s^{-1} was current dependent. This eliminates electrical fluctuations as a source of dark counts. The critical current as a function of the magnetic field was measured in the voltage-bias mode via the long coaxial cable with an additional low pass filter. The critical current was defined as the maximum in the CV curves. At the critical current, we typically found a rate of dark counts of 10^7 to 10^8 s^{-1} and a voltage of a few microvolts in excess of the zero-resistance value.

III. EXPERIMENTAL RESULTS

A. Critical current in magnetic field

We begin with the critical parameters of the superconducting state, which provide scales for measured critical currents and applied fields. The depairing critical current in straight portions of the square spiral was computed in the framework of the standard Ginzburg-Landau (GL) approach with the Bardeen temperature dependence and correction for the extreme dirty limit as

$$I_C^{\rm dep}(T) = \frac{4\sqrt{\pi}\,(e^{\gamma})^2}{21\,\varsigma(3)\sqrt{3}}\,\frac{\beta_0^2\,(k_B\,T_C)^{\frac{3}{2}}}{e\,R_S\sqrt{D\,\hbar}}\,w\left[1-\left(\frac{T}{T_C}\right)^2\right]^{3/2} \times K(T/T_C), \quad (1)$$

where $K(t) = 0.66 \times (3 - t^5)^{0.5}$ is the analytical presentation of the correction [17], $R_S = 300\,\Omega$ is the square resistance of our films at 20 K, $D = 5 \cdot 10^{-5}$ m^2 s^{-1} is the typical diffusivity of normal electrons in our films [14,18], $\beta_0 = 2.05$ is the ratio of the energy gap at zero temperature to $k_B T_C$ [19], and w is the strip width. For the square spiral with $w = 110$ nm and $T_C = 11.8$ K, we obtained a depairing critical current of 129 μA at $T = 4.2$ K.

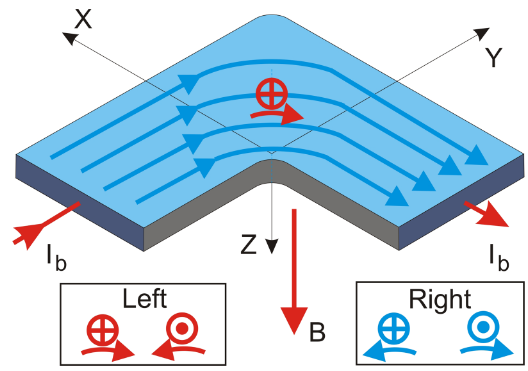

FIG. 3. (Color online) Bend schematics and positive directions of the external magnetic field (B) and bias current (I_b). These directions obey left field-current symmetry for which an increase in the magnetic field causes the increase in the superconducting current density at the inner corner of the bend. Pictograms in the left box denote two possible configurations that produce this effect. Pictograms in the right box denote configurations having right symmetry and, consequently, opposite effect on the current density at the inner corner. The pictogram in the bend corresponds to the positive directions of the field and current shown in the figure. The inner corner has coordinates (0; 0; 0) in the system shown here. It will be used through the paper.

The second critical magnetic field $B_{C2} = 13.3$ T at 4.2 K was computed with the following expression

$$B_{C2}(T) = \frac{2\sqrt{2}\,k_B\,T_C}{\pi\,e\,D}\left[1-\frac{T}{T_C}\right]\left[1+\frac{T}{T_C}\right]^{\frac{1}{2}}. \quad (2)$$

It is expected that, in a square spiral, current crowding [2] at the inner corners of bends will reduce the measured critical current of the whole spiral with respect to the critical current of its straight parts. External magnetic field induces screening current in bends. Depending on the field direction, the screening current may decrease or increase the local current density at the inner corners of bends [11]. Figure 3 shows a combination of field and current directions, which results in an increase of the local current density at the inner corner of a bend. The sign of the effect remains unchanged when both field and current directions are changed to the opposite. We will call the direction combinations, which have such an effect on the current density, the combination with the left field-current symmetry. Two pictograms in the left box depict two combinations with the left symmetry. The crosses or points in the circles denote two opposite directions of the magnetic field and the arrows denote the directions of the bias current in the bend. The other two combinations will be called combinations with the right field-current symmetry. The corresponding two pictograms are shown in the right box. We will be using pictograms through the paper to relate experimental data on plots to specific combinations of field and current directions.

In order to visualize the expected effect of the magnetic field on the current density, we computed in the framework of the GL formalism [20] the local density of superconducting current in a bend without a magnetic field and at a field of

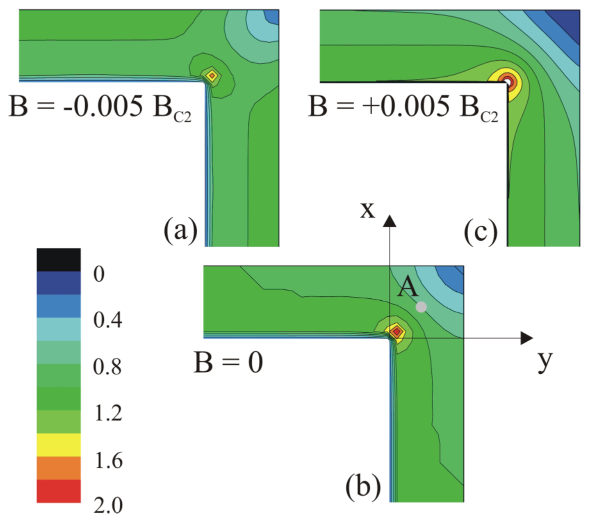

FIG. 4. (Color online) Density of the superconducting current in the bend and in the adjacent straight parts of a strip (b) without magnetic field and for the field $0.005 B_{C2}$ with (c) the positive and (a) negative directions. The current density is normalized to its density far from the bend at $B = 0$. The current distribution was computed for the strip width of 20ξ where $\xi = 5$ nm is the coherence length for our NbN films [14,18]. A gray circle labeled with the letter A in the common bisector of the bend corners [panel (b)] marks the position where the local current density does not change with the magnetic field.

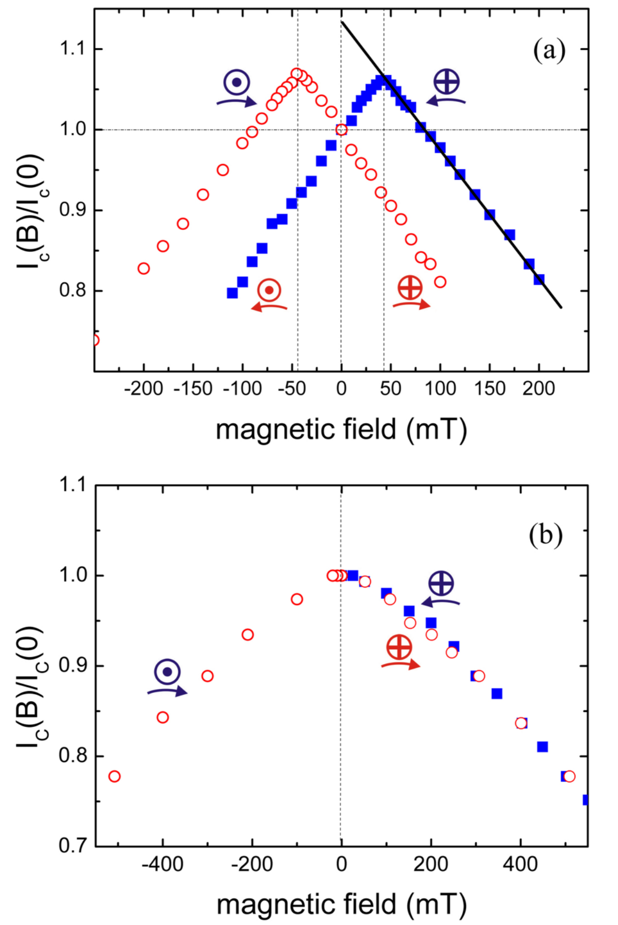

FIG. 5. (Color online) (a) Relative critical current of the square spiral in magnetic field for positive (open symbols) and negative (closed symbols) current directions. Pictograms depict combination of the field and current directions for each section of the plot. Solid straight line extrapolates to zero field the linear decrease of the critical current with the magnetic field in the right symmetry. Vertical dashed lines show zero field and positions of the maxima on the field axis. (b) Relative critical current of the circular spiral for different current directions. The same convention is used to mark symmetries and current directions.

$B = \pm 0.005\, B_{C2} = 66$ mT. The results are shown in Fig. 4 as two-dimensional contour plots. The critical current is achieved when either the vortex barrier at the inner corner disappears [2,4] or the local current density at the inner corner equals the depairing current density [21]. In both cases, one expects the critical current to decrease with an increasing field for the left field-current symmetry and to increase for the right field-current symmetry.

The critical current was measured for all possible combinations of field and current directions as a function of the magnetic field. The results are shown in Fig. 5 for (a) the square spiral and (b) the circular spiral. The square spiral demonstrates dependences expected for a single bend. For combinations with the right symmetry, the critical current increases with the field, reaches a maximum at $B_{\max} = 44$ mT, and further decreases. For combinations with the left symmetry, the critical current linearly decreases with the magnetic field. This effect was already reported for separate bends [12,13]. Simultaneous change of current and field directions mirrors the $I_C(B)$ curves with respect to the $B = 0$ line. Circular spirals do not show any asymmetry of the critical current in the magnetic field. Assuming that all bends in square spirals are identical, we apply the analysis of Ref. [13] to find, via linear extrapolation of the field dependence for the right symmetry, the critical current in the straight parts $I_{C0} = 42\,\mu$A and the reduction factor $R = I_{Cm}/I_{C0} = 0.86$ due to current crowding. Here, I_{Cm} is the maximum experimental critical current in the magnetic field. The critical current in straight parts of the spiral is less than the computed depairing current. The difference is within the range found for nanowires with similar stoichiometry [14]. The self-field that is produced by the critical current in the middle part of our spirals is less than 0.1 mT, which is from two to three times larger than the local earth magnetic field and almost two orders of magnitude less than typical $B_{\max}$ values.

B. Dark counts

The rate of dark counts in the square spiral is not symmetric with respect to the direction of either magnetic field or current. The minimum in the magnetic field dependence of the DCR appears for the same right field-current symmetry as the maximum in the magnetic field dependence of the critical current. This is illustrated in Fig. 6, where the DCR is plotted as function of the magnetic field for two opposite directions of the bias current. Like the critical current, the DCR is invariant for changing simultaneously both field and current directions. Noticeably, the minimum in the DCR occurs at a field of approximately 25 mT, which is smaller than the

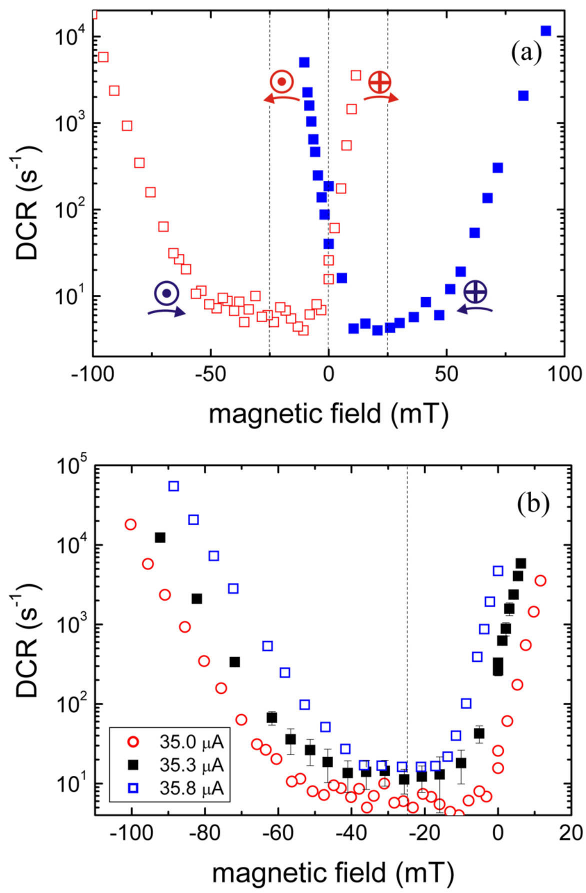

FIG. 6. (Color online) (a) Rate of dark counts in magnetic field for two directions of the bias current with the magnitude 35 μA. The DCR for the positive current direction is shown with open symbols and for the negative direction with closed symbols. Pictograms depict combination of the field and current directions for each section of the plot. Dashed vertical lines are to guide the eyes; they show field positions of the minima in the DCR and zero field. (b) Magnetic field dependencies of the DCR for different positive bias currents. Values of the bias current are specified in the legend. Vertical dashed line shows the location of the minimum on the field axis.

field corresponding to the maximum in the critical current. Increasing the bias current does not affect the position of the minimum in the DCR, but makes it more pronounced and sharp [Fig. 6(b)]. In circular spirals, the DCR was found symmetric with respect to field and current directions for any fields and currents.

C. Photon counts

Although, similar to the DCR, the rate of light counts exhibits an asymmetry separately with respect to field and current directions, the effect of field and current appears more complicated. First, the strength of asymmetry in the photon count rate (PCR) depends on the photon energy. Figure 7 shows the rate of photon counts in the magnetic field for three wavelengths: (a) 1400, (b) 800, and (c) 500 nm, and different bias currents. As reported earlier [7], the change in the PCR, which is produced by the same magnetic field, decreases with the decrease in the wavelength and varies from two orders of magnitude for the wavelength $\lambda = 1400$ nm to tens of a percent for $\lambda = 500$ nm. For each wavelength, an increase in the bias current reduces the amount of PCR variation in the magnetic field. Although, like the DCR, PCR is also invariant

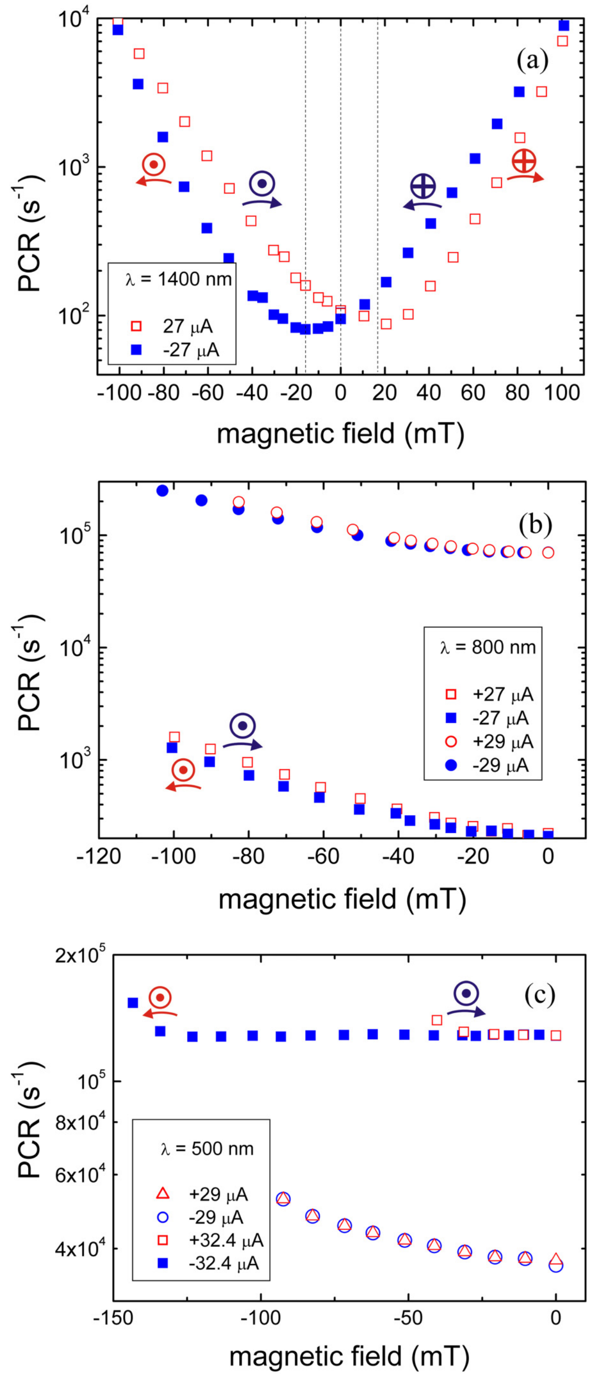

FIG. 7. (Color online) Rate of light counts in magnetic field for different wavelengths: (a) 1400 nm, (b) 800 nm, and (c) 500 nm. Magnitudes and directions of the bias current are specified in the legends. Conventionally, the PCR for the positive current direction is shown with open symbols, and closed symbols correspond to the negative direction. Vertical dashed lines in the panel (a) guide the eyes to the locations of the minima in the PCR on the field axis. Pictograms depict combinations of the field and current directions for each section of plots.

for simultaneously changing the directions of both field and current, the asymmetry in the PCR qualitatively differs from the asymmetry in the DCR. Remarkably, the minimum in the PCR appears for the left field-current symmetry [Fig. 7(a)] and not for the right symmetry, as it is found for the DCR. In other words, for the same current direction, the minimum in the PCR is shifted in the opposite direction on the field axis as compared to the minimum in the DCR. We will discuss this counterintuitive behavior at the end of this section. The absolute values of the field at the PCR minima for $\lambda = 1400$ nm are approximately 17 mT, which is less than the absolute field values at the DCR minima. The asymmetry in the PCR is more pronounced for large wavelengths and small currents and disappears completely for wavelengths smaller than approximately 600 nm. For the wavelength 800 nm and the bias current 27 μA, the asymmetry is still distinguishable [Fig. 7(b)], whereas it is already hard to see at a bias current of 29 μA. Within our experimental accuracy, we did not find any asymmetry for the wavelength of 500 nm [Fig. 7(c)]. The upturn in the plots for the bias current of 32.4 μA occurs when the critical current in the field decreases to the bias current. We did not find any asymmetry in the PCR dependences on the magnetic field for the circular spirals.

The effect of an external magnetic field on the critical current and rates of dark and light counts, which we described above, makes it possible to come to certain conclusions without invoking the qualitative microscopic analysis. Excluding a large single defect somewhere at the strip edge in the square spiral, we have to accept that any dark or light count event, whose rate is asymmetric with respect to the direction of either field or current alone, comes from the bends in the spiral. For the critical current, the field effect was already demonstrated in experiments on single-bended strips [12,13]. The maximum of the experimental critical current in magnetic field is achieved when increasing critical current in the bend equals decreasing critical current in the straight parts of the strip. For count events in a straight strip, any microscopic model would predict symmetric field or current dependencies of corresponding rates because the strip itself and the absorption probability for photons are both symmetric over the midline of the strip, and the distributions of the current density and the magnetic field in the strip have even and odd symmetry, respectively, with respect to the midline. Hence, when the field or current direction changes, this will not affect the critical current and count rates, which should remain unchanged. The square spiral consists from straight strips and bends. Therefore, any asymmetry may come from bends only. Indeed, in circular spirals where no sharp corners are present and the rounding radius of the spiral is much larger than the strip width, we did not observe any asymmetry. Furthermore, a weak asymmetry in the DCR with respect to the field direction has been recently observed in meanders [5] that contain turns with a different symmetry in small but nonequal numbers. Here, the net asymmetry may arise from a slight difference between geometrical shapes of individual turns.

The phenomenological explanation of the asymmetry in the DCR is straightforward. For the left symmetry of the field-current directions, the field increases the current density at the inner corner of each bend in the square spiral. This reduces the potential barrier for vortices entering the bend from the inner corner and, correspondingly, increases the rate of dark counts. The field applied in the right symmetry decreases the current density at the inner corner and decreases the count rate. When the field in the right symmetry further grows, the current density at the outer edges of straight strips increases and reduces the barrier for antivortices. At some field, they begin to dominate the net count rate, and the DCR starts to increase. Somewhere at an intermediate magnetic field, the DCR drops to a minimum. Since the rate of events from straight segments is symmetric with respect to the field direction and has a different field dependence as compared to the rate of events from bends, the net rate may have the minimum at a field smaller than the field that maximizes the critical current.

Intuitively, one would expect the same kind of asymmetry for the rate of light counts. However, this expectation silently postulates that light and dark counts undergo the same microscopic scenario. This is not necessarily the case. Recently, it has been found that the microscopic scenario of photon detection as well as the detection efficiency may differ locally [8,10,22]. Let us consider the point on the common bisector of both corners in the bend close to its midline, e.g. point A in Fig. 4(b). In the absence of an external field, the current density at the selected point is less than at the inner corner. The photon that is absorbed at this point creates a hotspot. The hollow in the order parameter forces the supercurrent to flow around and increases velocity of the condensate at the edges of the hotspot [8]. An external field in the left symmetry will decrease the current density locally around the hotspot. The photon is counted as a light event if either the velocity locally reaches the critical value and a VAP appears or a vortex enters the hotspot from any side and then moves to the opposite one. Hence, an increasing field either disables VAP appearance or increases the barrier for the vortex around the hotspot. The local PCR decreases either way. Obviously, the field applied in the opposite direction causes an increase in the local PCR. The net effect crucially depends on the distribution of the photon absorption probability in the bend and on the bias current. In the next section, we show that the two-dimensional GL model qualitatively explains different asymmetries in dark and light count rates.

IV. THEORETICAL MODEL

We first discuss critical currents in square spirals. We found the critical current, i.e. the current at which the superconducting state becomes nonstable, from the numerical solution of the GL equations [20] in the geometry shown in the inset in Fig. 8. We separately considered bends (B) where we neglect rounding, and straight segments of the strip with edge defects (A). The results are presented in Fig. 8 separately for the bend and for the straight segment. We found that the maximum of the critical current in the bend (closed symbols in Fig. 8) should occur for the right symmetry at $B \approx 0.02\, B_{C2} \approx 260$ mT. This is almost twice as large as the value obtained with the London model (Eq. (17) in Ref. [11]) for a sharp 90° bend. Taking into account nominal rounding of inner corners in bends of our structures $r/w = 0.65$ and assuming that all bends are identical, we expect in the framework of the London model a reduction factor of $R = 0.75$ (Fig. 14 in Ref. [2]) for the critical current

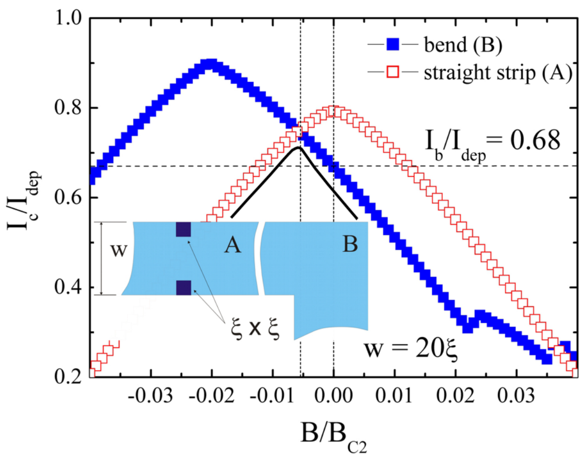

FIG. 8. (Color online) Relative critical current at different magnetic fields for the sharp bend in the strip with the width $w = 20\xi$ (closed symbols) and for the straight part of such a strip with defects (open symbols). The inset shows the geometry used for modeling: A, fragment of a straight strip with defects (not in scale); B, sharp bend. Solid line underlines currents that appear as critical currents of a spiral consisting from bends and straight strips. Vertical lines guide eyes to zero field and to the expected maximum in the critical current of the whole spiral. Horizontal line shows the bias current that was applied to measure the DCR [Fig 6(a)].

in bends and the maximum in the experimental critical current at $B_{\max} = 65$ mT (Eq. (17) in Ref. [11]). Our experimental values $R = 0.86$ and $B_{\max} = 44$ mT (Fig. 5) are reasonably close to predictions of the London model. Moreover, for our experimental reduction factor $R = 0.86$, the London model predicts $B_{\max} = 38$ mT, which even better corresponds to our experimental value $B_{\max} = 44$ mT. We attribute the remaining difference between the experimental reduction factor and the predicted factor, which is expected for a nominal rounding in our structures, to geometrical nonuniformities of the strip edges. Such nonuniformities typically appear as a result of ion etching [23]. They slightly decrease the effective width of strips in straight segments and increase the effective rounding radius of inner corners in bends.

To describe within the GL approach the reduction of the critical current in straight segments of the spiral, we introduced two identical defects at the opposite edges of our model strip (Part A of the inset in Fig. 8). Both defects represent a local suppression of the order parameter in an area $\xi \times \xi$ adjacent to the strip edge. They reduce the critical current in the straight strip to 80% of the depairing critical current in the strip of the same width without defects. The dependence of the critical current in the strip with defects on the magnetic field is shown in Fig. 8 with open symbols. The critical current of the spiral, which is composed of bends and straight strips, will be limited to the smallest value of the critical currents of these two components. The solid line in Fig. 8 shows the path that the critical current of the model spiral should follow with a varying magnetic field. In accordance with our experimental data, the maximum in the critical current occurs at ≈50 mT. It corresponds to the intersection of curves for the bend and for the straight strip. We understand that our experimental dependence of the critical current on the magnetic field can be modeled by a different set of rounding radii in the bend and the size of defects in the straight parts, e.g. smaller defects and a larger rounding radius. Since we cannot visualize defects, the set that we used to obtain our model currents is rather arbitrary. However, we do not anticipate any effects of this choice on the asymmetry in the rates of light and dark counts in magnetic fields.

Although dark counts are generated everywhere in the spiral, the rates per unit length (local DCR) depend crucially on the ratio between the local critical current and the bias current. The local DCR is proportional to $\exp(-\delta F/(k_B T))$ where δF is the local height of the barrier for vortex entry. In the framework of the London model for large bias currents $I_b \leqslant I_C$, the barrier scales with the difference between the local critical current and the bias current $\delta F \propto \delta I = I_C(B) - I_b$ [9]. Therefore, for fields $B > 0.005 B_{C2}$, the local DCR in bends will be much higher than the local DCR in straight strips. The total DCR in the spiral will depend on the relative weight of bends and straight strips. However, since the local DCR in strips is symmetric with respect to the direction of the magnetic field, the presence of any asymmetry in the magnetic field dependence of the total DCR ensures the nonvanishing contribution of bends to the generation of dark counts. To quantitatively compare our experimental results with the model calculations, we identify the depairing current in the GL model with the critical current in the straight strips in a zero magnetic field. Taking into account a 20% reduction of the model critical current in straight strips due to defects, we arrive at $I_b/I_{\rm dep} = 0.68$ for the bias current, which we used for the DCR measurements. This relative bias current is marked with the straight dashed line in Fig. 8. If bends noticeably contribute to the total DCR, one would expect a minimum in the total DCR at a field close to our experimental value of $B_{\max}$. Plots in Fig. 6(b) confirm this expectation. There is a minimum in the DCR around −30 mT. Slopes of the DCR versus magnetic field are different for fields with right symmetry at $B < -50$ mT (fewer dark counts from bends) and for fields with left symmetry at $B > -10$ mT (more dark counts from bends). Different slopes correspond to different weights of bends and straight segments in the total DCR. Since the bends do not dominate in the total DCR at all magnetic fields, the minimum in the field dependence of the DCR does not coincide with the maximum in the $I_C(B)$ dependence [compare Fig. 5(a) and Fig. 6(a)].

Accepting the thermally activated vortex crossing as the dominant photon-detection mechanism, one would expect for the PCR the same type of asymmetry as for the DCR. Indeed, the vortex should enter the superconductor and hotspot via the weakest place, i.e. the place where the current density/supervelocity is maximal. This can be the inner corner of the bend, especially when the hotspot is located close to it and the field of the left symmetry favors the entrance of a vortex with the same polarity as in the case of dark counts. However, contrary to dark count events, in the light count scenario, the vortex should also exit the hotspot. The local value of the order parameter inside the hotspot Δ is less than the equilibrium value $\Delta_{\rm eq}$ outside of the hotspot. If the relative local decrease of the order parameter is small $\delta = (\Delta_{\rm eq} - \Delta)/\Delta_{\rm eq} \ll 1$, the hotspot cannot pin the vortex, and it freely crosses the strip. When the relative decrease is large, the hotspot pins the vortex and prevents the light count. Whichever of these two occurrences holds for a particular order parameter in the hotspot depends on the bias current. In Fig. 9, we plot the current at which the vortex leaves the hotspot as a function of the location of the hotspot in the bend. We call this current the detection current $I_{\rm det}$ since it ensures the light count. Calculations are made in the framework of the modified hotspot model [24] with the radius of the hotspot $R = 5\xi$ and the relative reduction of the order parameter $\delta = 0.4$.

One can see that, close to the inner corner, there is an area in the bend where the small field of the left symmetry increases $I_{\rm det}$ while the field of the right symmetry decreases $I_{\rm det}$. This area is marked schematically in gray in the inset of Fig. 9(a). Positions on the cut through this area at $y = w/4$ are circled in Fig. 9(a). Here, they span over the interval of bias currents $0.42 I_{\rm dep} < I_b < 0.49\, I_{\rm dep}$. For any relative bias current within this interval, only the part of the circled area where $I_{\rm det} < I_b$ provides light counts. This active part decreases if a small positive (left symmetry) magnetic field is applied and increases if a magnetic field is negative (right symmetry). Because of the uniform and constant photon flux, the light count rate increases with the increase in the area that is collecting photons. Hence, the active part will deliver the PCR with the asymmetry, which we observed experimentally. This asymmetry is inverted with respect to the "normal" asymmetry of the DCR.

Note that, in the active part, the negative magnetic field favors exiting from the hotspot of the vortices that have entered the hotspot from the side of the inner corner. At the outer edge of the hotspot, far from the inner corner, the negative magnetic field increases the current density (and supervelocity) locally and decreases the energy barrier for vortex exit. The inverted asymmetry exists only in small magnetic fields. This corresponds to our experimental observation. The PCR at $\lambda = 1400$ nm becomes symmetric for fields larger than 100 mT [Fig. 7(a)]. The inverted asymmetry disappears for $\delta = (\Delta_{\rm eq} - \Delta)/\Delta_{\rm eq} > 0.5$, which corresponds to photons with higher energy. In this case, $I_{\rm det}$ in the bend and in the straight strip are practically equal. The inverted asymmetry also disappears when the hotspot loses its ability to pin vortices, e.g. when $\delta < 0.3$. At bias currents larger than $I_{\rm det}$ in straight strips, light counts come mostly from straight strips, and the PCR becomes symmetric.

Under the same conventions as for dark counts, we find that the current 27 μA, which we used to measured the PCR at $\lambda = 1400$ nm, corresponds to the model-relevant relative bias current $I_b = 0.5 I_{\rm dep}$. This current is at the upper boundary of the current interval where the inverted effect exists. However, since our choice of the rounding radius and the size of defects for the model dependence of the critical current on the field is not unique (see discussion above), the relative bias current may have a different value. In other words, we are not able, within the present model, to estimate numerically the relative weight of bends in the total rate of light counts.

We are aware that the analysis [25] based on the solution of the time-dependent GL equations has shown that light counts generated by bends differ from those originating from straight strips. More specifically, the overall duration of a PCR voltage pulse is smaller when the count comes from the bend and, at

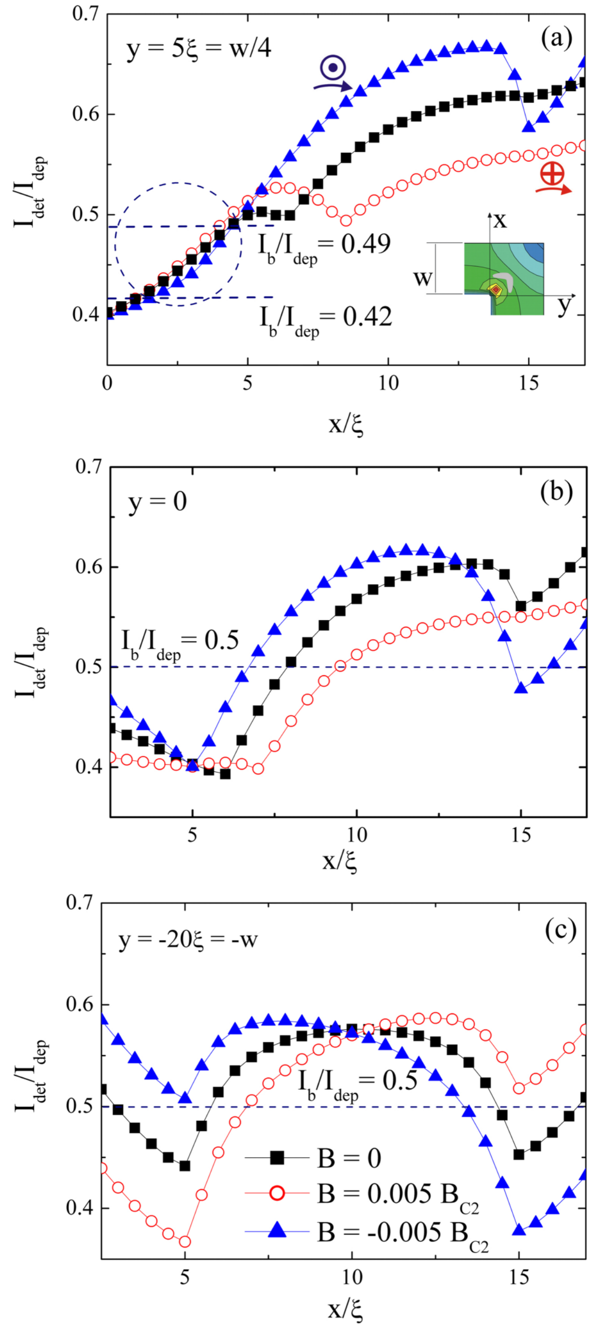

FIG. 9. (Color online) Detection current as a function of the positions (x) of the hotspot at three different distances [(a) $y = w/4$; (b) $y = 0$; (c) $y = -w$] from the inner corner of the bend without magnetic field and for the magnetic field $B = 0.005\, B_{C2}$ with opposite directions. Positive magnetic field corresponds to the left symmetry. Coordinate system is shown in the inset in the panel (a). The inset in panel (a) sketches the bend and the area (gray spot) where $I_{\rm det}$ is increased/decreased by small magnetic field of the left/right symmetry. The cut through this area at $y = w/4$ is marked with a blue dashed circle in the panel (a). Horizontal straight lines in panel (a) show boundaries for bias currents within which the effect exists. Horizontal lines $I_b = 0.5\, I_{\rm dep}$ in panels (b) and (c) show the nominal value of the bias current used to measure the PCR for the wavelength 1400 nm [Fig. 7(a)].

small bias currents, the amplitude of a PCR pulse from the bend is also smaller than the amplitude of the pulse from the straight strip. A recent paper based on the same theoretical approach [26] predicts a similar difference between the amplitudes of PCR voltage pulses originating from bends and straight strips with constrictions. With our spirals, we observe PCR and DCR pulses with equal mean amplitudes and an amplitude spread, which is much narrower than both models predict. The time resolution of the present experiment (approximately 100 ps) does not allow us to resolve the passage of kinematic vortices. Early experiments on meander structures, which include 180° turnarounds, had demonstrated a difference between mean amplitudes of PCR and DCR pulses as well as a decrease in the mean amplitude of PCR pulses with an increase of the photon energy [27]. These early observations contradict the results of both models. The reason for this discrepancy is not clear at this time. As in the case of dark counts, the asymmetry in the PCR itself ensures a noticeable contribution of the bends to the total rate of light counts.

We believe that the time-dependent GL equation alone cannot provide correct (quantitative) description of this problem. Without solving coupled GL and kinetic equations, it is not possible to state unambiguously whether the passage of a single Abrikosov vortex or a series of kinematic vortices leaves enough heat to create a normal resistive domain. Instead of the kinetic equation, authors of the both models [25,26] solved the heat conductance equation. This approach is only qualitatively valid because the time for vortex nucleation is smaller than the electron-electron inelastic relaxation time, and the usage of the effective temperature is not justified. Furthermore, the local heating by a photon was reduced in the model of Ref. [25] by the choice of the coefficient, which describes heat transfer from electrons to phonons. Its value was larger than the typical value in NbN films. With a more realistic value for this coefficient [26], one finds that the photon absorbed near the bend creates a normal domain at a smaller current than that required for generating light count in the straight strip.

V. DISCUSSION AND CONCLUSION

Theoretical considerations presented in the previous section are based on a relatively simple microscopic model of the hotspot [24]. The actual profile of the order parameter in the hotspot may differ from the assumption of this model that will quantitatively influence the pinning ability of a hotspot and the detection current. Furthermore, we cannot precisely relate the bias current in the experiment to the particular relative bias current in the GL model. Therefore, the contribution to the net PCR from different parts of the bend remains largely undefined. For the bias current $I_b = 0.5 I_{\rm dep}$, the hotspot positions around the geometric border between the bend and the straight strip [$y = 0$, Fig. 9(b)], which contribute to the net PCR, occupy an even larger area than the active positions in the central part of the bend. The positions at $0 < x/\xi < 5$ contribute with inverted asymmetry, whereas positions at $5 < x/\xi < 10$ contribute with normal asymmetry. The straight strips contribute symmetrically to the PCR at any bias current. Therefore, they smear out the shift of the minimum in the PCR to either side. The net PCR from all these areas may well be symmetric or show slight asymmetry.

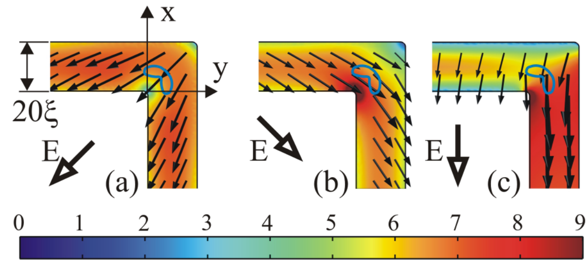

FIG. 10. (Color online) Relative probability of photon absorption in the bend and adjacent portions of the straight strips for the wavelength 1400 nm and different polarizations. Red (dark) color corresponds to the largest local probability. Blue curved lines circle the area that delivers the PCR with the inverted asymmetry. Black arrows show directions of currents that are excited in the bends by continuous electromagnetic waves. Polarization directions of the incident waves are shown with the empty arrows.

This interplay of light counts from different parts of the spiral is further modified by the probability of photon absorption. We computed this probability for plane waves with three different polarizations. We identified the probability of the photon absorption at a particular location with the relative density of the high-frequency current, which is induced in the structure by the plane wave at normal incidence. Simulations were carried out with the software COMSOL [28], which uses the finite-element method. To verify that the simulation results were not affected by numerical instabilities or similar problems, we compared the results obtained with COMSOL to similar simulations done with the software Lumerical [29]. The latter is based on the finite-difference time-domain method. The results provided by these two techniques almost coincide. The COMSOL software solves numerically Maxwell's equations in the frequency domain. The spiral is modeled by its specific geometry and is represented by its frequency dependent dielectric function. The calculations lead to an accurate theoretical treatment of the problem, and the results automatically include surface plasmons if they are excited. Therefore, no further separate analysis of surface plasmons is necessary. In all simulations, a maximum mesh size of 7 nm and a complex dielectric function for our NbN films in the normal state [30] were used. By comparing simulation results for a separate strip with a bend with the results for the whole spiral, we confirmed that there was no crosstalk between adjacent strips via evanescent fields. The results are shown in Fig. 10 as grayscale plots. They present relative current density in the equatorial surface of the bend at the frequency of the incident wave. For polarizations along the x or y axis [Fig. 10(c)], approximately half the bend is active in absorbing photons. The absorption probability is evenly distributed between hotspot positions, providing light count rates with different asymmetries. The polarization at 45° is seen differently by adjacent bends. The two possibilities are shown in Figs. 10(a) and 10(b). The polarization along the bisector [Fig. 10(a)] delivers more photons to positions, providing normal asymmetry; whereas photons with perpendicular polarization [Fig. 10(b)] are more strongly absorbed at positions, providing inverted asymmetry. The net effect of the absorption probability on the asymmetry in the PCR seems to be very weak. Therefore, we did not attempt to convolve the map of the absorption probability with the map of detection currents.

In this paper, we have demonstrated that, in structures that include bends with single symmetry, the rates of light and dark count events are asymmetric with respect to the direction of the external magnetic field and, separately, to the direction of the current. We have proven that this asymmetry is associated with the asymmetry of the current crowding in the bends. Applying a simplified microscopic GL model, we have shown that count events, which provide asymmetry, come from bends while the rate of events coming from straight strips remains symmetric with respect to field and current directions. The microscopic scenario of the light count event with intermediate pinning of the magnetic vortex in the hotspot explains the faint effect of the inverted asymmetry in the count rate for low-energy photons at small fields and currents. We have shown that, at large magnetic fields and currents, the asymmetry in the rate of light counts disappears as it is predicted by our theoretical model.

ACKNOWLEDGMENTS

D.Yu.V. acknowledges support from the Ministry of Education and Science of the Russian Federation (State Contract No. 02.B.49.21.0003) and from the Russian Foundation for Basic Research (Project No. 15-42-02365/15); I.C., K.D., and N.B. acknowledge support from Karlsruhe School of Optics and Photonics of Karlsruhe Institute of Technology (Project No. DFG GSC 21).

[1] C. M. Natarajan, M. G. Tanner, and R. H. Hadfield, Supercond. Sci. Technol. **25**, 063001 (2012).
[2] J. R. Clem and K. K. Berggren, Phys. Rev. B **84**, 174510 (2011).
[3] H. Bartolf, A. Engel, A. Schilling, K. Ilin, M. Siegel, H.-W. Hübers, and A. Semenov, Phys. Rev. B **81**, 024502 (2010).
[4] L. N. Bulaevskii, M. J. Graf, C. D. Batista, and V. G. Kogan, Phys. Rev. B **83**, 144526 (2011).
[5] A. Engel, A. Schilling, K. Ilin, and M. Siegel, Phys. Rev. B **86**, 140506(R) (2012).
[6] M. K. Akhlaghi, H. Atikian, A. Eftekharian, M. Loncar, and A. H. Majedi, Opt. Express **20**, 23610 (2012).
[7] R. Lusche, A. Semenov, Y. Korneeva, A. Trifonov, A. Korneev, G. Goltsman, and H.-W. Hübers, Phys. Rev. B **89**, 104513 (2014).
[8] A. N. Zotova and D. Yu. Vodolazov, Supercond. Sci. Technol. **27**, 125001 (2014).
[9] L. N. Bulaevskii, M. J. Graf, and V. G. Kogan, Phys. Rev. B **85**, 014505 (2012).
[10] A. Engel and A. Schilling, J. Appl. Phys. **114**, 214501 (2013).
[11] J. R. Clem, Y. Mawatari, G. R. Berdiyorov, and F. M. Peeters, Phys. Rev. B **85**, 144511 (2012).
[12] O.-A. Adami, D. Cerbu, D. Cabosart, M. Motta, J. Cuppens, W. A. Ortiz, V. V. Moshchalkov, B. Hackens, R. Delamare, J. Van de Vondel, and A. V. Silhanek, Appl. Phys. Lett. **102**, 052603 (2013).
[13] K. Ilin, D. Henrich, Y. Luck, Y. Liang, M. Siegel, and D. Yu. Vodolazov, Phys. Rev. B **89**, 184511 (2014).
[14] D. Henrich, S. Dörner, M. Hofherr, K. Il'in, A. Semenov, E. Heintze, M. Scheffler, M. Dressel, and M. Siegel, J. Appl. Phys. **112**, 074511 (2012).
[15] K. S. Il'in, D. Rall, M. Siegel, and A. Semenov, Physica C **479**, 176 (2012).
[16] K. Il'in, D. Rall, M. Siegel, A. Engel, A. Schilling, A. Semenov, and H.-W. Hübers, Physica C **470**, 953 (2010).
[17] M. Yu. Kupriyanov and V. F. Lukichev, Fiz. Nizk. Temp. **6**, 445 (1980) [Sov. J. Low Temp. Phys. **6**, 210 (1980)].
[18] A. Engel, A. Aeschbacher, K. Inderbitzin, A. Schilling, K. Ilin, M. Hofherr, M. Siegel, A. Semenov, and H.-W. Hübers, Appl. Phys. Lett. **100**, 062601 (2012).
[19] U. Pracht, E. Heintze, C. Clauss, D. Hafner, R. Bek, D. Werner, S. Gelhorn, M. Scheffler, M. Dressel, D. Sherman, B. Gorshunov, K. Ilin, D. Henrich, and M. Siegel, IEEE Trans. Terahertz Sci. Technol. **3**, 269 (2013).
[20] M. Tinkham, *Introduction to Superconductivity* (McGraw-Hill, New York, 1996).
[21] D.Yu. Vodolazov, Phys. Rev. B **85**, 174507 (2012).
[22] J. J. Renema, Q. Wang, R. Gaudio, I. Komen, K. op't Hoog, D. Sahin, A. Schilling, M. P. van Exter, A. Fiore, A. Engel, and M. J. A. de Dood, Nano Lett. **15**, 4541 (2015).
[23] K. Ilin, M. Siegel, A. Semenov, A. Engel, and H.-W. Hübers, Phys. Status Solidi C **2**, 1680 (2005).
[24] D. Yu. Vodolazov, Yu. P. Korneeva, A. V. Semenov, A. A. Korneev, and G. N. Goltsman, Phys. Rev. B **92**, 104503 (2015).
[25] G. R. Berdiyorov, M. V. Milosevic, and F. M. Peters, Appl. Phys. Lett. **100**, 262603 (2012).
[26] A. N. Zotova and D. Yu. Vodolazov, Supercond. Sci. Technol. **26**, 075008 (2013).
[27] P. Haas, A. Semenov, H.-W. Hübers, J. Beyer, A. Kirste, T. Schurig, K. Il'in, M. Siegel, A. Engel, and A. Smirnov, IEEE Trans. Appl. Supercond. **17**, 298 (2007).
[28] http://www.comsol.com (2012).
[29] http://www.lumerical.com (2012).
[30] A. Semenov, B. Günther, U. Böttger, H.-W. Hübers, H. Bartolf, A. Engel, A. Schilling, K. Ilin, M. Siegel, R. Schneider, D. Gerthsen, and N. A. Gippius, Phys. Rev. B **80**, 054510 (2009).